Electronic Supplementary Information (ESI)

Electrokinetics of pH-regulated zwitterionic polyelectrolyte nanoparticles

Li-Hsien Yeh,[1] Yi-Hsuan Tai,[2] Nan Wang,[2,3] Jyh-Ping Hsu,[2,*] and Shizhi Qian,[4,5*]

[1]Department of Chemical and Materials Engineering, National Yunlin University of Science and Technology, Douliou, Yunlin 64002, Taiwan

[2]Department of Chemical Engineering, National Taiwan University, Taipei, 10617, Taiwan

[3]College of Chemistry and Chemical Engineering, Huazhong University of Science and Technology, Wuhan, 430074, P.R. China

[4]Institute of Micro/Nanotechnology, Old Dominion University, Norfolk, VA 23529, USA

[5]School of Mechanical Engineering, Yeungnam University, Gyongsan 712-749, South Korea

* Corresponding authors:

E-mails: jphsu@ntu.edu.tw (Jyh-Ping Hsu), sqian@odu.edu (Shizhi Qian)

---

1. Effects of counterion condensation and double-layer polarization

The occurrence of counterion condensation (CC) is illustrated in Fig. S1, where the variations of the dimensionless net equilibrium concentrations of cations, $(c_{1e}+c_{2e})/C_{\mathrm{KCl}}$, and anions, $(c_{3e}+c_{4e})/C_{\mathrm{KCl}}$, as a function of r^* for two levels of molar concentration of acidic functional groups N_A are presented. This figure shows that due to CC, counterions (cations) are attracted into the interior of the polyelectrolyte (PE) nanoparticle (NP) and coions (anions) are expelled out from it. The higher the N_A the more significant CC phenomenon is.

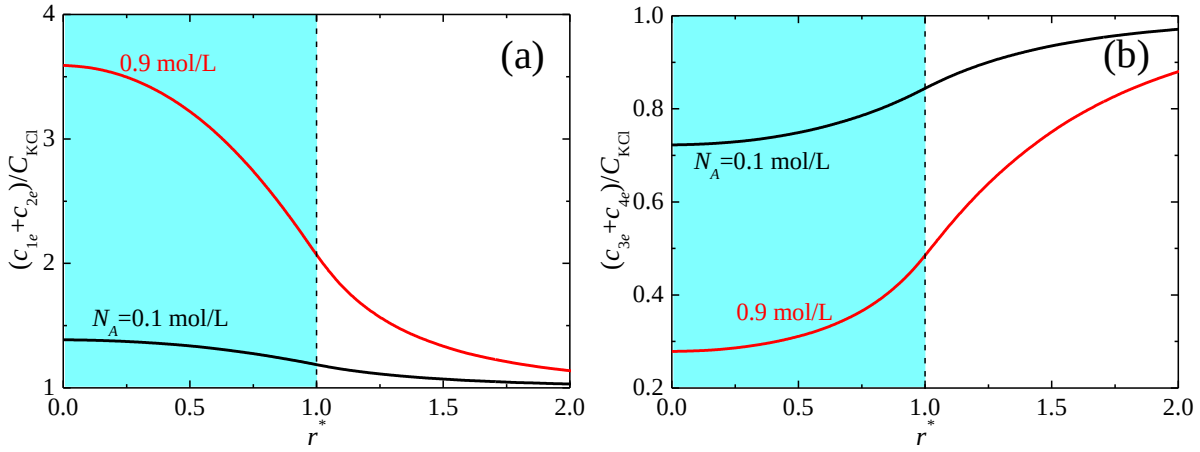

Fig. S1. Variations of the scaled net equilibrium concentrations of cations, $(c_{1e}+c_{2e})/C_{\mathrm{KCl}}$, (a), and anions, $(c_{3e}+c_{4e})/C_{\mathrm{KCl}}$, (b), as a function of $r^*(=r/a)$ near a PE NP for two levels of N_A at $C_{\mathrm{KCl}}=10\,\mathrm{mM}$ and $\mathrm{pH}=8$. Other conditions are the same as those in Fig. 7 of the text. The blue region highlights the interior of the PE NP.

Fig. S2a shows the dimensionless net perturbed ionic concentration, $[(\delta c_1+\delta c_2)-(\delta c_3+\delta c_4)]/C_{\mathrm{KCl}}$, where $\delta c_j=c_j-c_{je}$ with c_j and c_{je} being the molar concentration of ionic species *j* in the presence and absence of **E**, respectively, along the axis of the applied electric field at $\theta=0$ for two levels of N_A. Due to double-layer polarization (DLP) effect arising from the convective motion of the ionic species inside double layer, $[(\delta c_1+\delta c_2)-(\delta c_3+\delta c_4)]/C_{\mathrm{KCl}}$ is positive (negative) near the bottom (top) region of the PE NP, yielding an induced electric field, $\mathbf{E}_{\mathbf{DLP}}$, the direction of which is opposite to **E**. As a result, the local electric field near the PE NP is weakened, as seen in Fig. S2b, so are the electric driving force and the particle mobility, as seen in Fig. 8d and 7b of the text, respectively. Fig. S2b also reveals that DLP effect is more significant when N_A is large and

the thickness of electric double layer (EDL) is comparable to the particle radius. The latter is expected, and the former is because the larger the N_A the more the amount of the fixed charge of PE, and therefore, the higher the corresponding electric potential, as seen in Fig. 3 and 4 of the text, respectively.

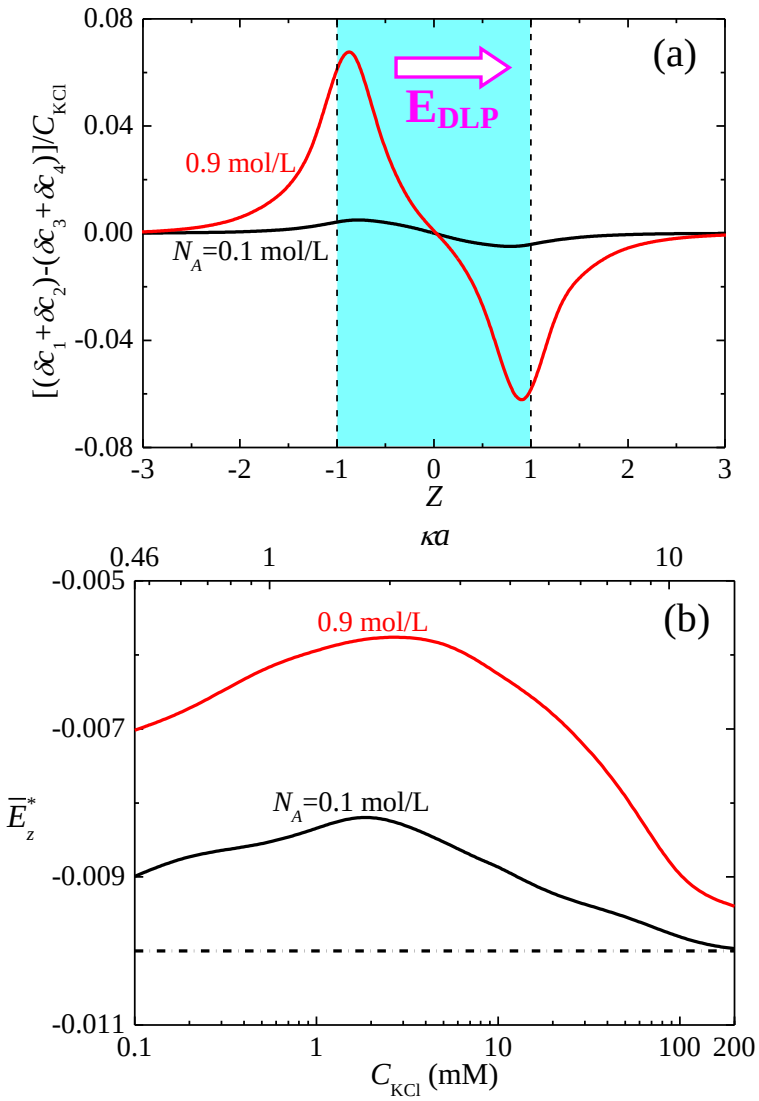

Fig. S2. (a) Variation of the scaled net perturbed ionic concentration, $[(\delta c_1+\delta c_2)-(\delta c_3+\delta c_4)]/C_{KCl}$, as a function of Z $(=z/a)$, the scaled distance along the direction of **E** at $\theta=0$ for two levels of N_A. Other conditions are the same as those in Fig. 7 at $C_{KCl}=1\,\mathrm{mM}$ and $\mathrm{pH}=10$. $\mathbf{E_{DLP}}$ denotes the induced electric field arising from the

DLP effect, the direction of which is opposite to that of the applied electric field. The blue region highlights the interior of the PE NP. (b) Scaled particle surface-averaged *z*-component local electric field, $\overline{E}_z^*$, as a function of background salt concentration C_{KCl} (and the corresponding κa) at two levels of N_A for the case of Fig. 7 at $\mathrm{pH}=10$. The dash-dotted line represent the scaled original strength of the applied electric field $E_z^*=0.01$, which is stronger than that in the other two cases due to the DLP effect.

2. Perturbed flow and pressure fields in subproblem two

Fig. S3 and S4 illustrate the influence of CC on the scaled *z*-component fluid velocity, v_z^* ($=v_z/U_r$), and the scaled perturbed pressure, δp^*, near the PE NP in subproblem two, respectively. As seen in Fig. S3, if N_A is small (lines with symbols) both the magnitude of v_z^* and its rate of strain across the PE NP surface increase with increasing deviation of pH from the IEP of the PE (i.e., 6). However, if N_A is large (lines) CC becomes significant. In this case, an appreciable amount of counterions are attracted into the interior of PE so that the distortion of the electroosmotic flow inside the PE NP by the applied electric field is alleviated. As a result, the rate of strain across the PE NP surface as pH deviates appreciably from IEP decreases, yielding a distinct perturbed pressure gradient field shown in Fig. S4. The less distorted electroosmotic flow leads to a smaller $\left|F_{h2(v)}^*\right|$, and the variation in the rate of strain across the PE NP surface makes $F_{h2(p)}^*$ positive, both of these result in a decrease in $\left|F_{h2}^*\right|$ $\left(=\left|F_{h2(v)}^*\right|+\left|F_{h2(p)}^*\right|\right)$. Note that if the deviation of pH from IEP is sufficiently large, F_{h2}^*

might change its sign from negative to positive, as shown in Fig. 9d of the text, due to the significant CC effect.

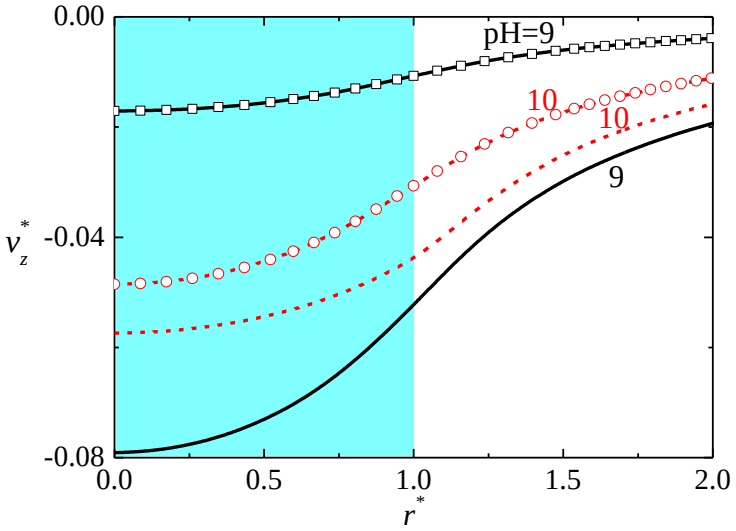

Fig. S3. Variation of the scaled *z*-component fluid velocity, v_z^*, at $\theta = 90°$ (perpendicular to the direction of the applied electric field) as a function of r^* near a PE NP in subproblem two at various combinations of N_A and pH for $C_{\mathrm{KCl}} = 100\,\mathrm{mM}$. Blue region: interior of PE NP; lines and lines with symbols: N_A=0.9 and 0.1 mol/L, respectively. Other conditions are the same as those in Fig. 7 of the text.

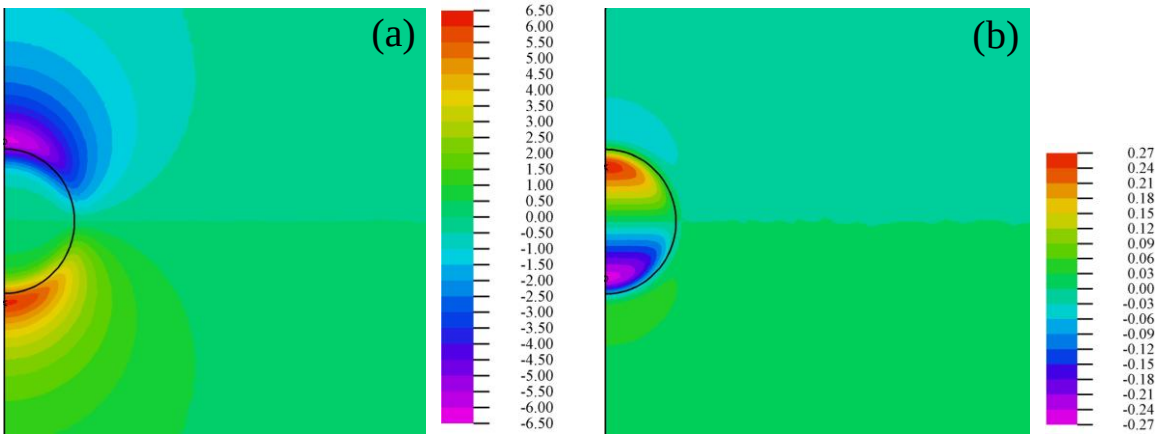

Fig. S4. Contours of the scaled perturbed pressure δp^* near a PE NP in subproblem two at pH=9, (a), and 10, (b), for $C_{\mathrm{KCl}} = 100\,\mathrm{mM}$. Other conditions are the same as those in Fig. 7d of the text.

3. Influence of softness parameter of a PE NP on scaled forces

The behaviors of μ^* seen in Fig. 10 a and b of the text are similar to those of F_2^* in Fig. S5a and b, respectively, implying that the behaviors of μ^* as C_{KCl} and pH vary are dominated mainly by the two competing forces, F_{e2}^* and F_{h2}^*. It is interesting to note in Fig. 10 of the text that the behavior of μ^* at large λa is distinctly different from that at small λa. This might result from that, in the case of large λa, both effects of DLP and CC are offset by the EOF of counterions. For example, as seen in Fig. S5a, $F_{h2}^*(\lambda a = 1) > 0$, and $F_{h2}^*(\lambda a = 30) < 0$. Therefore, F_{e2}^* is enhanced by a positive F_{h2}^* in the former, and offset by a negative F_{h2}^* in the latter, so that F_2^* and, therefore, μ^*, has a local minimum with increasing C_{KCl} in the former, and increases with increasing C_{KCl} in the latter. Similarly, the effect of CC, which yields an appreciable decrease in both $\left|F_{h2}^*\right|$ and $\left|F_2^*\right|$ for a loose-structured PE ($\lambda a = 1$) at a high level of pH (see the discussion in Fig. 7d of the text), is also offset by an increase in $\left|F_{h2}^*\right|$ for a compact-structured PE ($\lambda a = 30$), as can be seen in Fig. S5b. The behavior of μ^* (or F_2^*) seen in Fig. 10 of the text results mainly from that of F_{h2}^*, which is dominated by the EOF velocity profile inside the EDL (or the corresponding $F_{h2(v)}^*$). As illustrated in Fig. S6, the PE NP is negatively charged when $\mathrm{pH} > \mathrm{IEP}$ and, therefore, the direction of the corresponding EOF is in the same direction as that of the electric field imposed. For a loose-structured PE NP (lines with symbols in Fig. S6), the fluid flow driven by the imposed electric field and the equilibrium electric field can

penetrate easily through it. In this case, the rate of strain across the PE NP surface is positive, so are $F^*_{h2(v)}$ and F^*_{h2}, as seen in Fig. S5. On the other hand, it is uneasy for fluid flow to penetrate a compact-structured PE NP, and the rate of strain across its surface becomes negative, as seen in Fig. S6 (lines), so are $F^*_{h2(v)}$ and F^*_{h2}, as shown in Fig. S5. It is interesting to note in Fig. S6b that for a loose-structured PE NP (lines with symbols), the magnitude of the rate of strain across its surface decreases with increasing deviation of pH from the IEP. As discussed in Fig. 7d of the text, this is due to the effect of CC. However, for a compact-structured PE NP (lines), that magnitude increases with increasing deviation of pH from the IEP, resulting in an increase in $\left|F^*_{h2(v)}\right|$ (and therefore, F^*_{h2}), as shown in Fig. S5b and c. This is because although a considerable amount of counterions is condensed inside a compact-structured PE NP when CC is significant, the fluid inside it is nearly stationary so that the maximum fluid velocity occurs at a point outside it, as shown in Fig. S6b.

The influence of the scaled softness parameter of the PE NP, λa, on the corresponding scaled forces, F^*_{e2}, F^*_{h2}, F^*_2, $F^*_{h2(v)}$, and $F^*_{h2(p)}$ acting on it for the case of Fig. 10 in the text are depicted in Fig. S5. As seen in Fig. S5a, if λa is small (i.e., 1), F^*_2 shows a local minimum as C_{KCl} increases; however, if it is large (i.e., 30), F^*_2 decreases monotonically with increasing C_{KCl}. The former can be attributed to the DLP effect, which results in a local minimum occurring at $C_{\mathrm{KCl}} \to 1\,\mathrm{mM}$ (i.e., $\kappa a \to 1$) as seen in Fig. S5a. The latter results from the competition between a positive F^*_{e2} and a negative F^*_{h2}. Note that $F^*_{e2}(\lambda a = 1)$ is

smaller than F_{e2}^{*} ($\lambda a = 30$). This is because the fluid flow is faster in the former, and therefore, the DLP effect arising from the convective motion of ionic species is more significant, yielding a smaller F_{e2}^{*}. The sign of F_{h2}^{*} can be explained by the combined effects of $F_{h2(v)}^{*}$ and $F_{h2(p)}^{*}$, as discussed in Fig. S6. Fig. S5b shows that if λa is small (i.e., 1), $\left|F_2^{*}\right|$ has a local maximum as pH deviates from the IEP of the PE NP. On the other hand, if λa is large (i.e., 30), $\left|F_2^{*}\right|$ increases monotonically with increasing deviation of pH from IEP. The behavior of $\left|F_2^{*}\right|$ at $\lambda a = 1$ can be attributed to the CC effect occurring at higher deviation of pH from IEP. This effect leads to a decrease in both $\left|F_{h2(v)}^{*}\right|$ and $\left|F_{h2(p)}^{*}\right|$ as pH deviates appreciably from IEP, and even makes the sign of $F_{h2(p)}^{*}$ to change from negative at a small pH deviation to positive at a large pH deviation, as seen in Fig. S5c. If the deviation of pH from IEP is sufficiently large, these effects result in a sudden decrease in $\left|F_2^{*}\right|$, as shown in Fig. 5b. The behavior of $\left|F_2^{*}\right|$ at $\lambda a = 30$ seen in Fig. 5b results from the competition between the oppositely signed F_{e2}^{*} and F_{h2}^{*}. For example, if pH>6, then $F_{e2}^{*} > 0$ and $F_{h2}^{*} < 0$. The negative F_{h2}^{*} is due to the combined effects of $F_{h2(v)}^{*}$ and $F_{h2(p)}^{*}$, both are negative, as shown in Fig. S5c. These negative values of $F_{h2(v)}^{*}$, $F_{h2(p)}^{*}$, and F_{h2}^{*} at $\lambda a = 30$ are dominated by the EOF profile near the PE NP, and can be explained by that the rate of strain of EOF across the PE NP surface changes its sign from positive (for a loose-structured PE NP at $\lambda a = 1$) to negative (for a compact-structured PE NP at $\lambda a = 30$), as shown in Fig. S6.

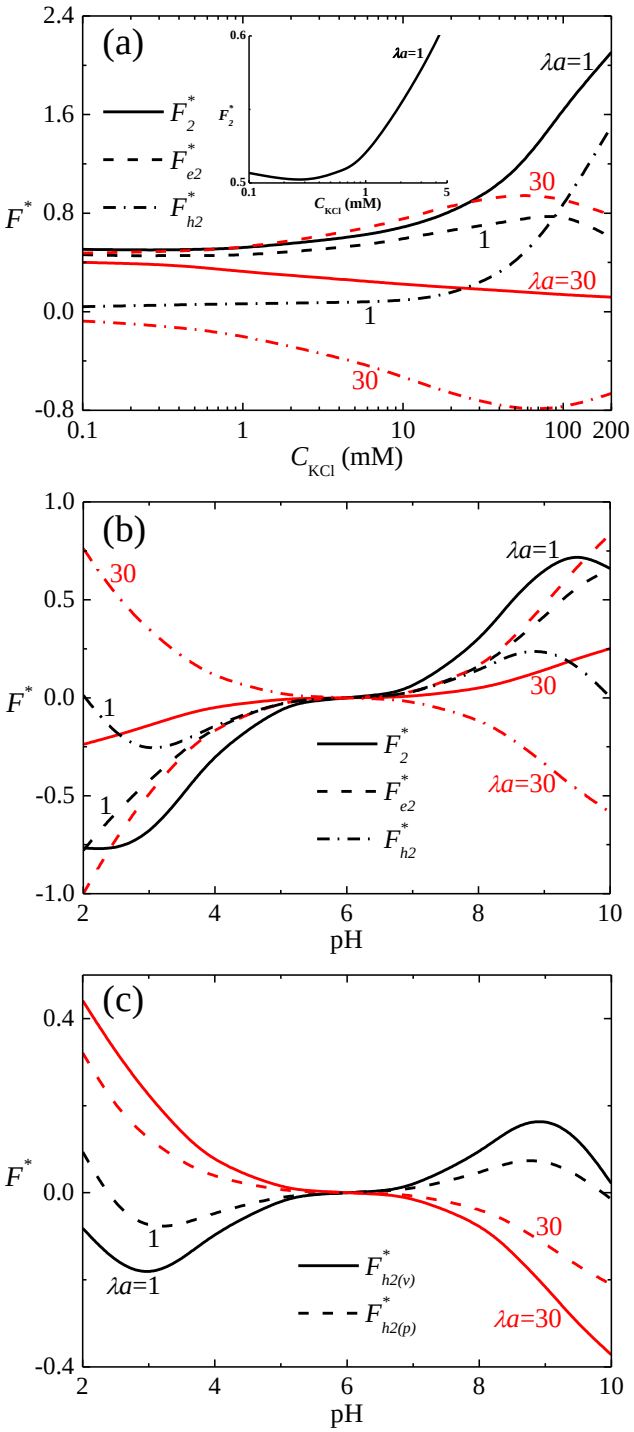

Fig. S5. Scaled forces in subproblem two, F_{e2}^*, F_{h2}^*, and F_2^* $(=F_{e2}^*+F_{h2}^*)$, as a function of C_{KCl}, (a), at two levels of λa for the case of Fig. 10a in the text, and as a function of pH, (b), for the case of Fig. 10b in the text. The inset in (a) is the enlarged region of F_2^* for the case of $\lambda a = 1$ at $0.1\,\mathrm{mM} \le C_{\mathrm{KCl}} \le 5\,\mathrm{mM}$. (c) Scaled viscous and pressure components of F_{h2}^*, $F_{h2(v)}^*$ and $F_{h2(p)}^*$, respectively, for the case of (b).

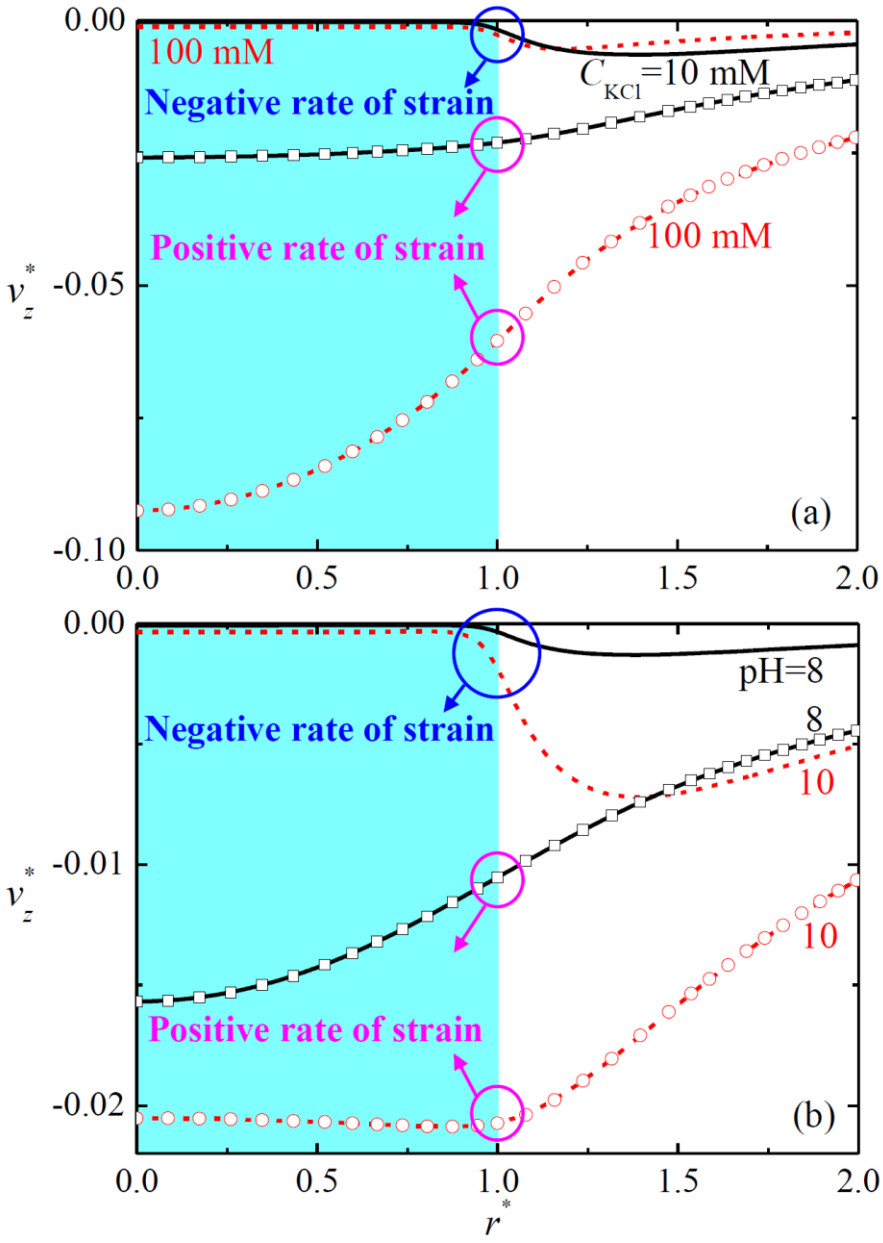

Fig S6. Variation of the scaled *z*-component fluid velocity, v_z^* $(=v_z/U_r)$, at $\theta=90°$ (perpendicular to the direction of the applied electric field) as a function of r^* near a PE NP in sub-problem two at various combinations of C_{KCl} and λa for the case of Fig. 10a in the text, (a), and at various combinations of pH and λa for the case of Fig. 10b in the text, (b). The blue region highlights the interior of PE NP. Lines and lines with symbols denote $\lambda a=30$ and 1, respectively.